ACS APPLIED MATERIALS & INTERFACES

Research Article

www.acsami.org

Discrepancy of Optimum Ratio in Bulk Heterojunction Photovoltaic Devices: Initial Cell Efficiency vs Long-Term Stability

Hyunmin Park,[†,§] Keel Yong Lee,[‡] Wanjung Kim,[†] Hee-Won Shin,[‡] Dong Hwan Wang,[†,⊥] Tae Kyu Ahn,*[,‡] and Jong Hyeok Park*[,†]

[†]School of Chemical Engineering and [‡]Department of Energy Science, Sungkyunkwan University, Suwon 440-746, Republic of Korea

Supporting Information

ABSTRACT: Organic photovoltaic devices are difficult to commercialize because of their vulnerability to chemical degradation related with oxygen and water and to physical degradation with aging at high temperatures. We investigated the photophysical degradation behaviors of a series of poly(3-hexylthiophene) (P3HT)/[6,6]-phenyl C61-butyric acid methyl ester ($PC_{60}BM$) bulk heterojunctions (BHJs) as a model system according to the donor−acceptor ratio. We found that the optimum P3HT:$PC_{60}BM$ ratio in terms of long-term stability differs from that in terms of initial cell efficiency. On the basis of cell performance decays and time-resolved photoluminescence measurements, we investigated the effects of oxygen and material self-aggregation on the stability of an organic photovoltaic device. We also observed the changes in morphological geometry and analyzed the surface elements to verify the mechanisms of degradation.

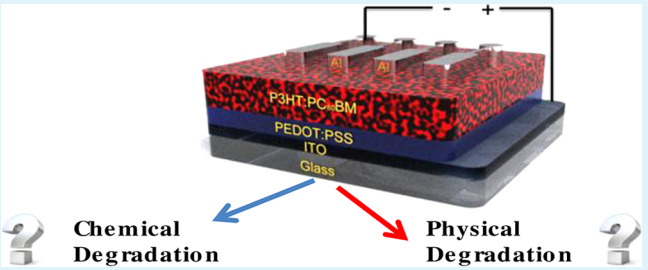

KEYWORDS: *organic solar cells, degradation, stability, bulk heterojunction, morphology, lifetime*

1. INTRODUCTION

Photovoltaic devices (or organic solar cells) based on conjugated polymers and fullerene derivatives used for sustainable electricity have been extensively researched and reported in recent years due to their cost effectiveness and wide-range application.[1−7] Device performances have been improved significantly by the efficient device structures of a bulk heterojunction (BHJ). Particularly, the BHJ structures have a high donor−acceptor interfacial contact area for efficient charge carrier separation, resulting in decreased charge carrier recombination.[8−19] Hence, controlling the morphology of the BHJ active layer is crucial in the optimization of cell performances.

In this BHJ structure, however, the nanostructural morphology is difficult to control. The morphology of the BHJ film is strongly dependent upon the fabrication conditions, such as the donor/acceptor mixing ratio, used organic solvent, additives, spin-casting speed, and thermal annealing conditions.[20,21] Especially, BHJ cells with P3HT and PCBM may achieve maximum power conversion efficiency by controlling the ratio between P3HT and PCBM and by changing the thermal annealing conditions.[22−25] Even if the resulting film morphology is optimized immediately after fabrication, the optimum morphology may be changed during a long-term cell operation under a high-temperature condition because this mixed BHJ structure is not the thermodynamically stable state.[26] The BHJ materials tend to aggregate as a result of self-aggegation, and thus unfavorable large-phase separation was observed.[27] This morphological change drastically lowers device performance. So, extensive research has been done on the aforementioned nanomorphology control of domains for long-term stability. In particular, morphological stability has been investigated through the use of compatibilizers,[28] cross-linkable polymers,[29] and block copolymers.[30]

Another possible reason for the device degradation is originated from air. For the organic solar cells that consist of fullerene as the acceptor semiconductor and are exposed to air, the most possible reason for cell instability was the decrease in C_{60} conductivity after oxygen and water absorption.[31,32] The oxygen and water absorption can form traps in the C_{60} layer that might also establish a space charge and therefore would decrease the exciton dissociation efficiency in the cells, resulting in severe degradation of the cell performance. However, little research has been done for finding degradation behaviors of conjugated polymer/fullerene derivative based photovoltaic devices until now.

Therefore, an investigation of the physical/chemical changes of an active layer aged under various controlled conditions (such as direct contact with air without temperature change or aging under high temperatures without air) can be meaningful in finding a way to improve the long-term stability of organic photovoltaic devices for their rapid commercialization.[33,34] In this study, the effects of the P3HT/PCBM ratio on the long-term stability of BHJ solar cells, which degrade under oxygen or argon atmosphere either at room temperature or at a high temperature, have been reported. Especially, we focus on the influence of the PCBM content in the BHJ layers on initial cell

Received: October 7, 2012
Accepted: February 11, 2013
Published: February 11, 2013

   dx.doi.org/10.1021/am302185f | ACS Appl. Mater. Interfaces 2013, 5, 1612−1618

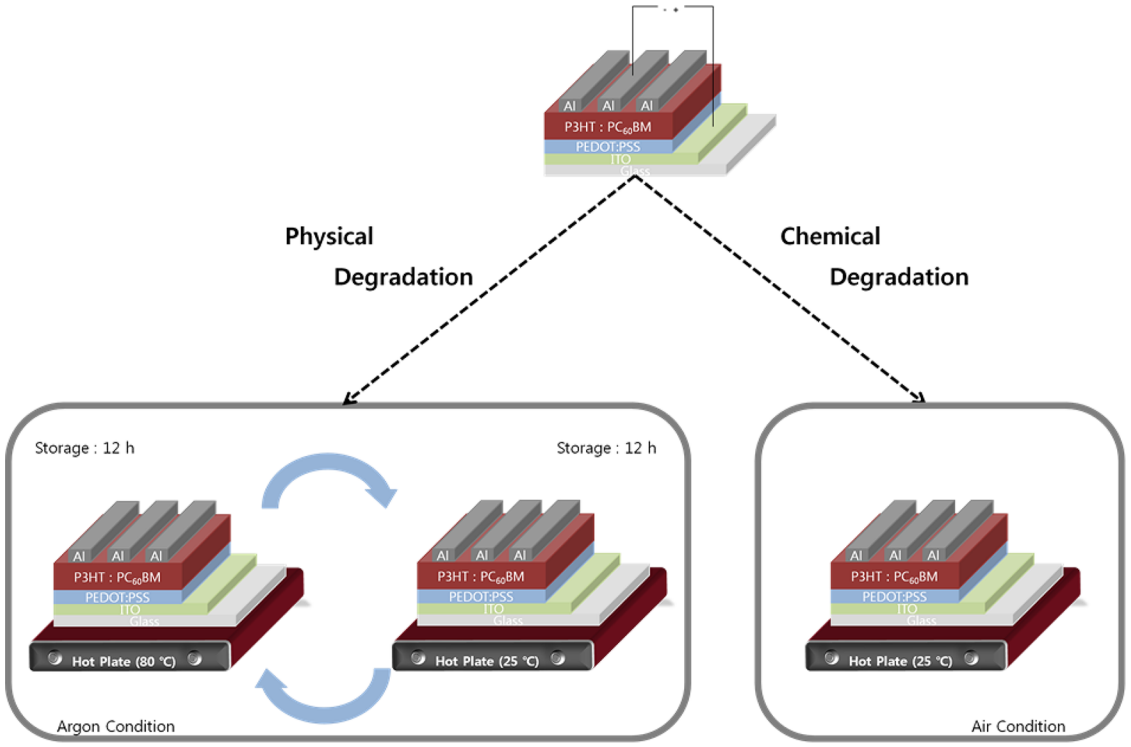

Figure 1. Schematic diagram of the device stability test structure.

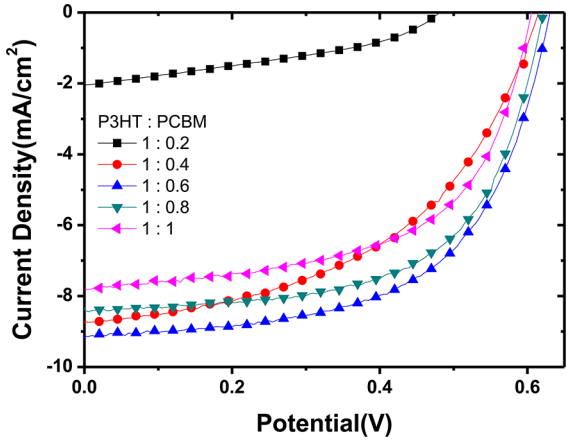

Figure 2. J–V characteristics of the initial state with various ratios (wt %) under 1 sun illumination (100 mW/cm^2).

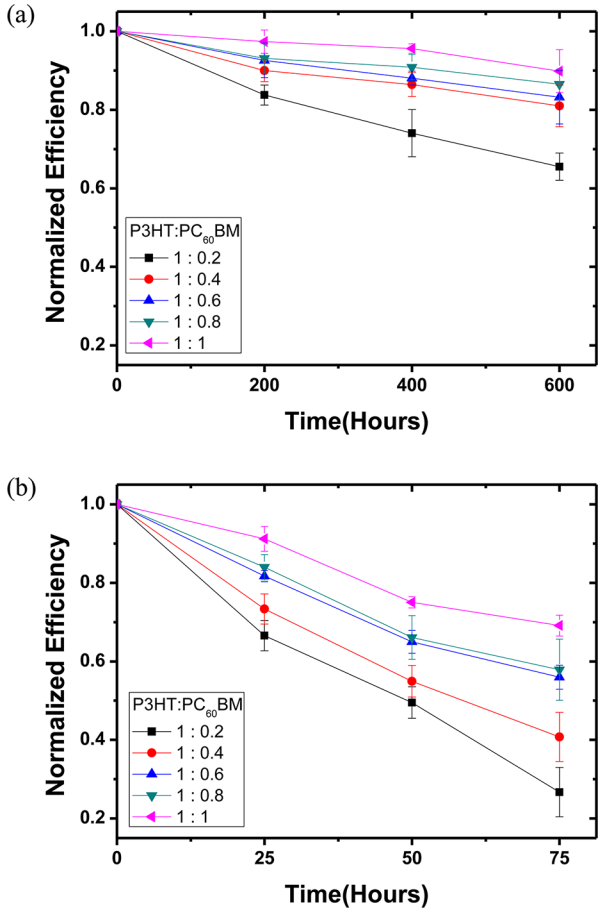

Figure 3. Normalized device efficiency at various ratios (wt %). (a) Alternating temperature change from 80 °C (12 h) to 25 °C (12 h) in argon over 600 h. (b) Storage at 25 °C over 75 h in air.

efficiency and long-term stability. To understand the degradation mechanism, we used a time-resolved PL technique, morphological analysis, and surface element analysis. The best composition for long-term stability differs from the composition of initial cell performance.

2. EXPERIMENTAL SECTION

Chemical Preparation. Regioregular P3HT (Sepiolid P100: ~95% regioregularity, 50 000 MW average molecular weight) was purchased from Rieke Metals, and PCBM (99.5% purity) was purchased from Nano-C. Mixtures with P3HT:PCBM weight ratios of 1:0, 1:0.2, 1:0.4, 1:0.6, 1:0.8, and 1:1 were prepared. The mixture was then poured into chlorobenzene and stirred for 19 h to dissolve in the solvent at room temperature (25 °C) in the argon condition.

Device Fabrication and Measurement. ITO-coated glass, which was used as a substrate, was washed by dipping in 2-propyl alcohol for 10 min, in acetone for 10 min, and in 2-propyl alcohol for another 10 min.

dx.doi.org/10.1021/am302185f | ACS Appl. Mater. Interfaces 2013, 5, 1612–1618

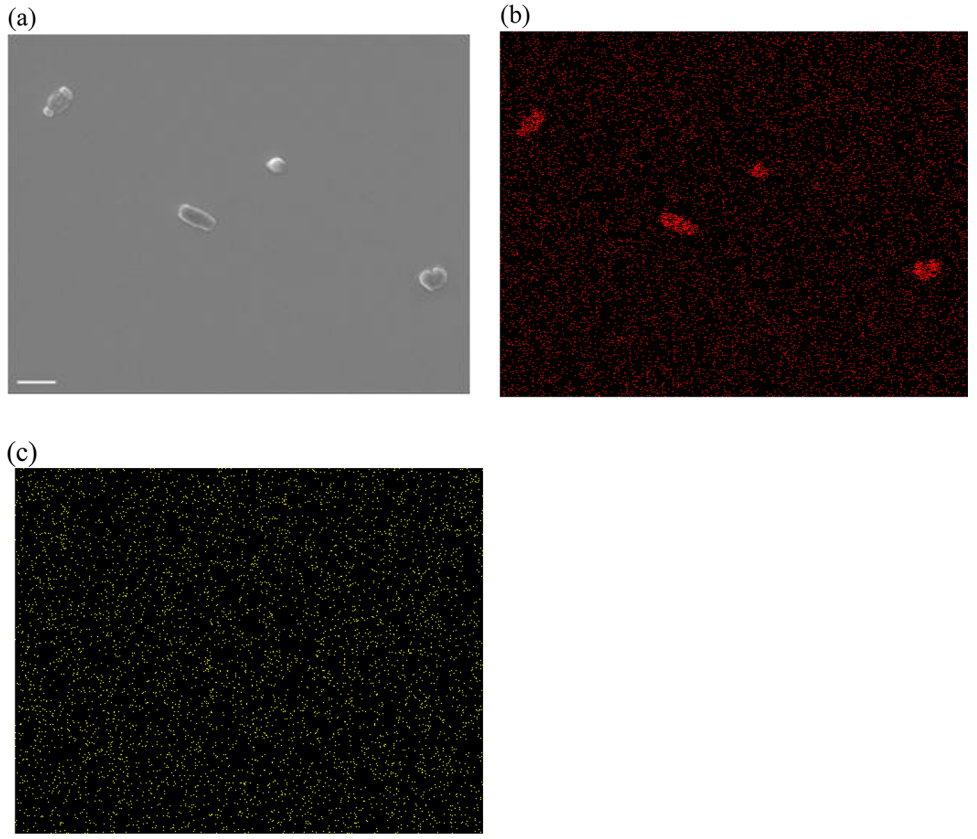

Figure 4. (a) Field emission scanning electron microscopy image of P3HT:$PC_{60}BM$ blended film after 24 h annealing at 150 °C in argon. (b) Carbon (C) element mapping corresponding to (a). (c) Sulfur (S) element mapping corresponding to (a). Scale bar = 10 μm.

Finally, the solvent was removed by blowing inert gas. The ITO substrate was then irradiated by UV light for 20 min before use. The hole transporting layer was formed by spin-casting poly(3, 4-ethylenedioxythiophene):poly(styrene sulfonate) (AI 4083) on the ITO glass and baking the layer at 115 °C for 15 min in air. The thickness of the layer that formed was 40 nm. The active layer of 110 nm thickness was then formed by spin-casting prepared solutions on the hole-transporting layer. A 100 nm Al cathode was thermally deposited on the active layer under vacuum pressure of 3×10^{-6} Torr before the cells were postannealed at 150 °C for 30 min in a glovebox filled with inert argon gas.

One of the photovoltaic devices was exposed to the 25 °C air condition for 75 h (hereafter chemical degradation); another set was stored in the argon condition for 600 h to protect against contact with oxygen and water. A sample was handled in two steps: an alternating temperature change from 80 to 25 °C, each step of which took 12 h (hereafter physical degradation). To measure $J-V$ characteristics of devices, the photovoltaic properties of the solar cells were measured using a Keithley model 2400 source measuring unit under 100 mW cm^{-2} illumination from a 1000 W Xenon lamp (Spectra-Physics) as the light source.

Characterization. Field emission scanning electron microscopy (FESEM, JSM700F, Japan) was used to analyze the sample morphology, and an energy dispersive spectrometer (EDS) was used to confirm the elements and their distribution. The FESEM image was obtained at 1000× magnification at 15.0 kV. A photoelectron spectrometer (Riken-Keiki) was used to measure the fluorescence of the sample. Time-resolved emission spectra and fluorescence intensity decays were obtained using a FluoTime200 system (Picoquant GmbH). The excitation sources were a light emitting diode (LDH-P-C-405B, 405 nm, 40 MHz repetition rate, Picoquant GmbH). TimeHarp300 TCSPC board (PicoQuant GmbH) was used for data processing. The laser was operated at a fixed 40 MHz repetition rate. For emission measurements, a monochromator was set to the 670 nm position. We used a Glan−Taylor polarizer at the magic angle position to obtain the lifetime data. The fluorescence intensity decay curves ($I(t)$) were analyzed using the FluoFit software (PicoQuant GmbH), which is based on a multiexponential model involving an iterative deconvolution process. Fluorescence decay is often a sum of the exponentials, where α_i and τ_i are the pre-exponential factor and fluorescence lifetime, respectively. The nanosecond transient absorption spectrum and time profiles were measured by a homemade nanosecond flash photolysis setup. Pump and probe light had 500 nm and 400−700 nm wavelengths, which were generated by the Optical Parametric Oscillator (OPO) powered by Quanta-Ray (INDI-40-10, SpectraPhysics) and the Xe lamp (LS-150-Xe, Abet Technology Inc.), respectively. The transmitted probe signal was selected through a monochromator (Acton 2300i, Princeton Instruments) obtained from a photomultiplier tube (Hamamatsu R928) and processed by a 500 MHz digital storage oscilloscope (DSO-X 3054A, Agilent Inc.).

3. RESULTS AND DISCUSSION

Figure 1 shows a schematic diagram of the device stability test that was performed on a P3HT/PCBM BHJ for a series of composition ratios as a function of storage time at 25 °C under air environment (chemical degradation) or an alternating temperature change from 80 °C (storage time: 12 h) to 25 °C (storage time: 12 h) under argon gas environment (physical degradation).[22] The alternate aging test was carried out at temperatures of 80 and 25 °C because the photovoltaic device was operated at a temperature of about 80 °C during the day and at 25 °C at night. The alternate aging test under argon atmosphere enabled us to differentiate the physical degradation of the devices from the oxygen-induced chemical degradation. Moreover, the aging test under the air condition at 25 °C can represent chemical degradation only. Figure 2 shows the curves

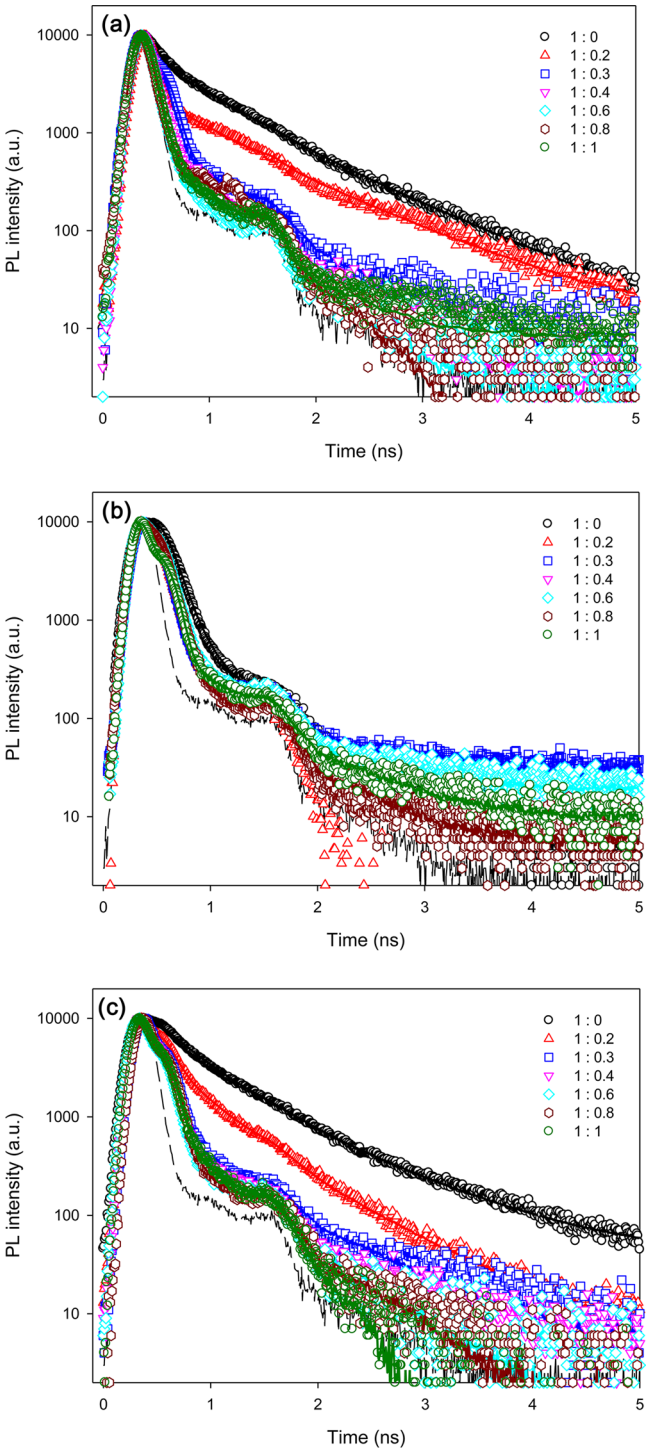

Figure 5. Time profiles of PL of pristine P3HT:PCBM blended film and P3HT:PCBM blended film with various ratios (wt %). (a) Pristine. (b) Storage at 25 °C over 75 h in air. (c) Alternating temperature change from 80 °C (12 h) to 25 °C (12 h) in argon over 600 h. All the PL traces are distinguished from the instrumental response function of ca. 150 ps at full width half-maximum and are convoluted well (dashed line). Details of convoluted PL lifetimes are listed in Table 1.

of current density versus potential ($J-V$) under AM 1.5G irradiation (100 mW/cm^2). Importantly as reported by M. Reyes-Reyes et al., the device made from a weight ratio of 1:0.6 had maximum efficiency.[22,23] As such, in terms of initial cell efficiency without any aging process, the solar cell devices with the donor−acceptor ratio of 1:0.6 had the best performance.

Figure 3 shows the normalized efficiency decay as a function of the P3HT:PCBM ratio when the devices were aged under the physical degradation pathway (Figure 3(a)) or the chemical degradation pathway (Figure 3(b)). Under both experimental conditions, more long-term stability was observed as the PCBM content increased in the active layer. The degradation mechanism of the active layer in the oxygen-free condition is well correlated with the morphological changes.[24,29,35]

As shown in Figure 3(a), the efficiences of the devices decreased as a function of the aging time under physical degradation. To compare the time-dependent efficiency decay of the solar cells with a series of acceptor weights, all cell efficiencies were normalized by their initial efficiencies. From the data, we realized that the device with the more acceptor (PCBM) content had more long-term stability. The device with the BHJ with 1:0.2 ratio showed not only the lowest initial cell efficiency but also the worst physical long-term stability among the cells with a series of acceptor weights. Because a device was stored in the inert Ar gas condition, the possibility of chemical degradation by air or water can be ignored. Donor−donor interaction may be considered the major degradation mechanism that can explain the results. To support this hypothesis, we have checked the morphological structures of a series of solar cells.[36] When the film consisting of P3HT and PCBM (1:1 by weight) was annealed thermally at 150 °C for 24 h, some aggregated PCBM was observed.[29] Figure 4(a) shows the aggregated PCBM on the surface of the P3HT/PCBM blended film. Mapping of the entire surface revealed that the aggregated part was mainly composed of carbon elements (Figure 4(b)). Findings in Figures 4(b) and 4(c) also indicated that the aggregated parts had higher carbon contents than other parts of the surface. Generation of the aggregated PCBM indicates that the excitons generated by the P3HT molecules could not be effectively separated into holes and electrons because the excitons were localized within their diffusion length, unable to contribute to the photocurrent. That is the main reason why all of the devices represented efficiency decays even under an oxygen-free environment.

Recently, several research groups characterized the nanomorphologies of BHJ by using transmission electron microscopy (TEM) images of the cross sections of the polymer and polymer:fullerene blended layers.[37−39] This technique is largely considered as one of the most promising techniques for monitoring the BHJ morphology using the P3HT/PCBM bilayer. However, the TEM image is questionable for the precise characterization of the morphological changes of the BHJ during the thermal annealing process. Time-resolved spectroscopy has been broadly used to monitor carrier dynamics in materials or chemical compounds. It measures the spectroscopic change of carrier, i.e., exciton, hole, electron, etc. Herein to investigate the charge separation efficiency of the cells between P3HT and PCBM in the BHJ, we measured the photoluminescence (PL) time profiles of a series of samples after a short excitation by a picosecond pulse. Using PL lifetime measurements, we can estimate the dynamics of charge separation in cells, and we can probe at which PCBM content the photophysical process of a cell can be optimal.[40] Figure 5(a) compares the fluorescence decay profiles of the BHJ films with different PCBM contents by the time-correlated single photon counting (TCSPC) technique.[41] Briefly, as the PCBM content of the BHJ film increased, the initial PL lifetime decreased, but the PL lifetime completely saturated in

dx.doi.org/10.1021/am302185f | ACS Appl. Mater. Interfaces 2013, 5, 1612−1618

Table 1. (a) PL Lifetimes of P3HT:PCBM Blended Films Immediately after Preparation, (b) PL Lifetimes of P3HT:PCBM Blended Films after 75 h under Air, and (c) PL Lifetimes of P3HT:PCBM Blended Films after 600 h under Argon

a								intensity average	amplitude average
P3HT/PCBM (wt ratio)	A1	τ_1 (ns)	A2	τ_2 (ns)	A3	τ_3 (ns)	χ^2	$\langle\tau\rangle$ (ns)	τ (ns)
1/0			0.7266	0.360	0.2734	0.934	1.162	0.6432	0.5165
1/0.2	0.8359	0.046	0.0875	0.370	0.0766	0.950	1.435	0.5763	0.1439
1/0.3	0.9829	0.045	0.0125	0.340	0.0046	0.950	1.087	0.1432	0.0528
1/0.4	0.9855	0.048	0.0140	0.361	0.0005	0.942	1.285	0.0858	0.0503
1/0.6	0.990	0.048	0.010	0.361			1.114	0.070	0.051
1/0.8	0.986	0.045	0.014	0.365			1.450	0.078	0.049
1/1.0	0.991	0.048	0.009	0.345			1.074	0.067	0.051
b								intensity average	amplitude average
P3HT/PCBM (wt ratio)	A1	τ_1 (ns)	A2	τ_2 (ns)	A3	τ_3 (ns)	χ^2	$\langle\tau\rangle$ (ns)	τ (ns)
1/0	0.998	0.117	0.002	0.950			1.221	0.130	0.118
1/0.2	0.994	0.066	0.006	0.774			1.002	0.115	0.070
1/0.3	0.998	0.057	0.002	0.960			1.221	0.081	0.059
1/0.4	0.999	0.060	0.001	0.930			1.017	0.072	0.061
1/0.6	0.885	0.063	0.115	0.114			1.046	0.072	0.068
1/0.8	0.981	0.057	0.019	0.110			1.149	0.059	0.058
1/1.0	0.998	0.041	0.002	0.917			1.095	0.078	0.043
c								intensity average	amplitude average
P3HT/PCBM (wt ratio)	A1	τ_1 (ns)	A2	τ_2 (ns)	A3	τ_3 (ns)	χ^2	$\langle\tau\rangle$ (ns)	τ (ns)
1/0			0.808	0.360	0.192	0.960	1.221	0.593	0.475
1/0.2	0.789	0.065	0.188	0.360	0.024	0.948	1.002	0.346	0.141
1/0.3	0.988	0.060	0.002	0.330	0.009	0.955	1.221	0.177	0.069
1/0.4	0.996	0.060			0.004	0.940	1.017	0.113	0.064
1/0.6	0.997	0.055			0.003	0.940	1.046	0.098	0.058
1/0.8	0.998	0.055			0.002	0.970	1.149	0.092	0.057
1/1.0	0.984	0.058	0.016	0.370			1.095	0.088	0.063

the cell with P3HT:PCBM = 1:0.4. The PL decay data were fitted using the following multiexponential function

$$I(t) = \int_t^0 \mathrm{IRF}(t') \sum_n^{i=1} A_i e^{-t-t'/\tau_i} dt'$$

where A_i is the amplitude of the ith decay, n the number of exponential decays involved, and τ_i the ith lifetime constant. For a reference cell of a pure P3HT film, the (intensity) averaged PL lifetime was 0.64 ns. When hole/electron charge separation occurs in a donor–acceptor cell after photoexcitation, the PL lifetime shortens due to quenching. A shorter PL lifetime of a donor–acceptor combined cell implies the faster carrier dynamics in BHJ cells resulting in the better efficiency of the cell. This is because the generated excitons in P3HT could be quenched by the charge separation process related to PCBM near P3HT. As shown in Figure 5(a), the PL lifetime reached the saturated minimum point at the 1 (P3HT):0.4 (PCBM) ratio. Solar cell performance is generally determined by the combination of the following processes: light absorption, exciton generation, charge transfer, and charge transport. So, from the perspective of charge separation of the donor–acceptor, the 1 (P3HT):0.4 (PCBM) ratio reaches the saturation point (Table 1a).

Figures 5(a) and (b) show the PL decays of BHJ films for a series of donor–acceptor compositions before and after physical degradation. We found that the PL lifetime of pure P3HT (0.64 ns) without thermal physical degradation was longer than those of the P3HT:PCBM blend systems, indicating that charge separation occurred at the interfaces between P3HT and PCBM. Interestingly, the exciton lifetime (0.59 ns) of the pure P3HT film decreased after the physical degradation test. Therefore, the thermal annealing process induced the molecular ordering of P3HT, resulting in increased intermolecular interactions (exciton–exciton interaction). The decreased lifetime of the excitons formed on P3HT can give it a much worse chance of encountering acceptor molecules. We also found that the PL lifetimes of the blend films before the physical degradation test were shorter than those of the films after the physical degradation test, resulting in an unfavorable morphology change. We believe that the unfavorable morphology change is actually a phase separation in the blend film, a finding that is in good agreement with the SEM observations. The decreased interfacial area between P3HT and PCBM leads to nonefficient charge separation.

To investigate the charge separated state directly, we considered the use of transient absorption spectroscopy, which uses a nanosecond laser pulse and a Xe lamp light as pump and probe sources, respectively. Figure 6(a) shows transient absorption spectra at 10 μs for the P3HT:PCBM blended films of 1:0, 1:0.4, and 1:1 ratios. As the concentration of the PCBM increased, the bleaching peak around 500 nm revealed a blue-shift which is consistent with steady-state absorption spectra (Figure 6a inset). Interestingly induced absorption bands at 420 nm of the blended samples indicated higher optical density (OD) than those of the pure P3HT film. We believe that the transient absorption at 420 nm is related to the charge separated states of the P3HT cation and PCBM anion. The thiophene cation spectrum was reported to show enhanced absorption around 400 nm.[42−44] The relaxation carrier dynamics of the blended films showed prolonged dynamics of 1.67 and 1.1 ms, which were ten times slower than the 0.16 ms kinetics of the pure P3HT films (Figure 6b, 6c, 6d). The enhanced lifetimes of the blended samples, which might be related to charge recombination processes, give better efficiency in a photovoltaic

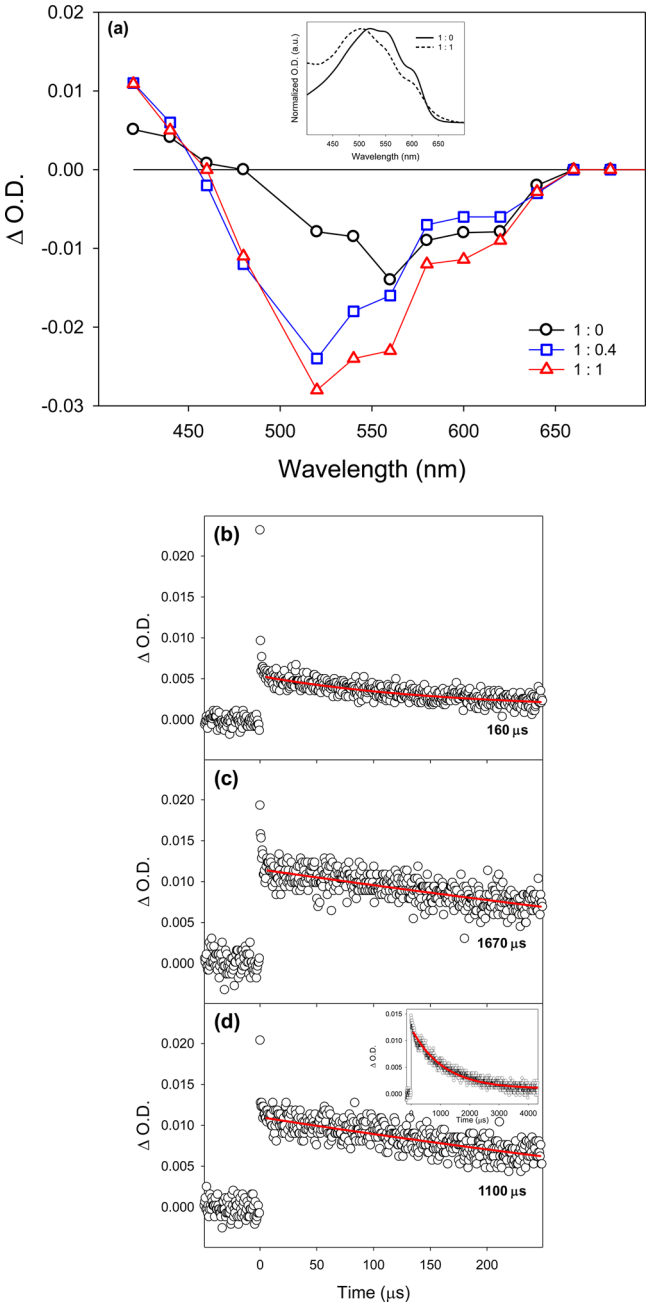

Figure 6. (a) Nanosecond transient absorption spectra of P3HT:PCBM blended films of 1:0, 1:0.4, and 1:1 (wt) at 10 μs time delay. Inset shows steady-state UV−vis spectra of pure P3HT and P3HT:PCBM (1:1 wt) film. (b),(c),(d) Denote time profiles of P3HT:PCBM blended films of 1:0, 1:0.4, and 1:1 (wt), repectively. The long component of decay times is described in each figure.

cell because losses of unwanted processes will be suppressed.[40] Interestingly, the film with weight ratio of 1:0.4 (P3HT:PCBM) showed slightly longer charge recombination time (1.67 ms) than the 1:1 film (1.1 ms) problably due to the PCBM aggregation.

Additionally, to obtain more information about the chemical degradation of the BHJ film, we performed TCSPC before and after the chemical degradation pathway (Figure 5(b)). Because a device was stored at room temperature, the possibility of physical degradation by morphology change can be ignored. To support this hypothesis, we have checked the morphological structures of the film with 1:1 ratio. As can be seen in Figure S1 (Supporting Information), there is no noticeable phase separation before and after the chemical degradatoin experiment for 75 h. We found that the PL lifetime of the pure P3HT film was greatly decreased after the chemical degradation experiment (Table 1b). We believe that the decreased lifetime was due to the formation of a quenching site, such as carbonyl moieties, sulfinic acids, and hydroxyl adducts.[41] P3HT:PCBM blend films after the chemical degradation pathway have exciton lifetimes not much different from their initial exciton lifetimes except the films with low PCBM content. For example, when the BHJ film with P3HT and PCBM (1:1 by weight) was degraded under the chemical degradation pathway, the exciton lifetime was decreased from 0.09 to 0.07 ns. Actually, this value is not much different from that of the chemically degraded pure P3HT film. Because the BHJ films were stored at room temperature, we can neglect the effect of a morphological change on lifetime change. Therefore, the generated excitons in the donor material may be consumed by the quenching site and not by the acceptor material, resulting in decreased photocurrent. As the content of PCBM is increased in the BHJ film, the possibility of exciton dissociation between the donor and the acceptor might increase, compared to that between the donor and the oxidized species, resulting in a slow decay of the cell performances.

4. CONCLUSIONS

We analyzed the stability of BHJ solar cells with various donor−acceptor ratios ranging from 1:0 to 1:1 (P3HT:PCBM by weight). In terms of initial cell efficiency, the BHJ film with the 1:0.6 (P3HT:PCBM by weight) composition showed the most efficient initial cell performance. However, in terms of device stability, the BHJ film with the 1:1 (P3HT:PCBM by weightt) composition showed better stability both in the physical degradation pathway and in the chemical degradation pathway. The high acceptor content in the BHJ film can minimize the negative effect of physical degradation from unwanted morphological changes and the negative effect of chemical degradation from the formation of oxidized species in the donor material, resulting in better device stability. These results suggest that the optimum composition between a donor and an acceptor should be reconsidered from the perspective of device stability according to the initial device efficiency.

■ ASSOCIATED CONTENT

Ⓢ Supporting Information

Field emission scanning electron microscopy image of P3HT:PC60BM blended film after 72 h stored at 25 °C in air. This material is available free of charge via the Internet at http://pubs.acs.org.

■ AUTHOR INFORMATION

Corresponding Author

*E-mail: lutts@skku.edu and taeahn@skku.edu. Tel.: 82-31-290-7346. Fax: 82-31-290-7272.

Present Address

[§]Green Energy Research Division, Daegu Gyeongbuk Institute of Science and Technology (DGIST), 50-1, Sang-ri, Hyeonpung-myeon, Dalseong-gun, Daegu 711-873, Republic of Korea.

[⊥]Center for Polymers and Organic Solids, University of California at Santa Barbara, Santa Barbara, California 93106-5090

Notes

The authors declare no competing financial interest.

■ ACKNOWLEDGMENTS

This work was supported by an NRF grants funded by the Korea MEST ((NRF-2009-C1AAA001-2009-0094157), the NCRC program (2011-0006268), and (2009-0092950)). T.K.A. acknowledges the support from the Global Frontier R&D Program (2011-0031565) and the New and Renewable Energy Program through the KETEP funded by the Ministry of Knowledge Economy (MKE) (008NPV08J010000).

■ REFERENCES

(1) Heeger, A. J. *Angew. Chem., Int. Ed.* **2001**, *40*, 2591−2611.
(2) Krebs, F. C.; Fyenbo, J.; Jørgensen, M. *J. Mater. Chem.* **2010**, *20*, 8994−9001.
(3) Liu, R. C. *J. Phys. Chem. C* **2009**, *113*, 9368−9374.
(4) Krebs, F. C.; Nielsen, T. D.; Fyenbo, J.; Wadstrøm, M.; Pedersen, M. S. *Energy Environ. Sci.* **2010**, *3*, 512−525.
(5) Winder, C.; Sariciftci, N. S. *J. Mater. Chem.* **2004**, *14*, 1077−1086.
(6) Dennler, G.; Scharber, M. C.; Brabec, C. J. *Adv. Mater.* **2009**, *21*, 1323−1338.
(7) Alstrup, J.; Jørgensen, M.; Medford, A. J.; Krebs, F. C. *ACS Appl. Mater. Interface* **2010**, *2*, 2819−2827.
(8) Thompson, B. C.; Fréchet, J. M. J. *Angew. Chem., Int. Ed.* **2008**, *47*, 58−77.
(9) Kim, H.; Shin, M.; Kim, Y. *J. Phys. Chem. C* **2009**, *113*, 1620−1623.
(10) Li, G.; Yao, Y.; Yang, H.; Shrotriya, V.; Yang, G.; Yang, Y. *Adv. Funct. Mater.* **2007**, *17*, 1636−1644.
(11) Wang, D. H.; Im, S. H.; Lee, H. K.; Park, J. H.; Park, O. O. *J. Phys. Chem. C* **2009**, *113*, 17268−17273.
(12) Yu, G.; Gao, J.; Hummelen, J. C.; Wudl, F.; Heeger, A. J. *Science* **1995**, *270*, 1789−1791.
(13) Yoon, S. J.; Park, J. H.; Lee, H. K.; Park, O. O. *Appl. Phys. Lett.* **2008**, *92*, 143504.
(14) Ma, W.; Yang, C.; Gong, X.; Lee, K.; Heeger, A. J. *Adv. Funct. Mater.* **2005**, *15*, 1617−1622.
(15) Helgesen, M.; Søndergaard, R.; Krebs, F. C. *J. Mater. Chem.* **2010**, *20*, 36−60.
(16) Li, G.; Shrotriya, V.; Huang, J.; Yao, Y.; Moriarty, T.; Emery, K.; Yang, Y. *Nat. Mater.* **2005**, *4*, 864−868.
(17) Schilinsky, P.; Asawapirom, U.; Scherf, U.; Biele, M.; Brabec, C. J. *Chem. Mater.* **2005**, *17*, 2175−2180.
(18) Chen, F. C.; Chien, S. C. *J. Mater. Chem.* **2009**, *19*, 6865−6869.
(19) Chien, S. C.; Chen, F. C.; Chung, M. K.; Hsu, C. S. *J. Phys. Chem. C* **2012**, *116*, 1354−1360.
(20) Yang, X. N.; van Duren, J. K. J.; Rispens, M. T.; Hummelen, J. C.; Janssen, R. A. J.; Michels, M. A. J.; Loos, J. *Adv. Mater.* **2004**, *16*, 802−806.
(21) Chirvase, D.; Parisi, J.; Hummelen, J. C.; Dyakonov, V. *Nanotechnology* **2004**, *15*, 1317−1323.
(22) Reyes, M. R.; Kim, K.; Dewald, J.; Sandoval, R. L.; Avadhanula, A.; Curran, S.; Carroll, D. L. *Org. Lett.* **2005**, *7*, 5749−5752.
(23) Reyes, M. R.; Sandoval, R. L.; Alatorre, J. A.; Alonso, R. G.; Carroll, D. L.; Martinez, A. L. *Thin Solid Films* **2007**, *516*, 52−57.
(24) Ho, C. S.; Huang, E. L.; Hsu, W. C.; Lee, C. S.; Lai, Y. N.; Lai, W. H. *Jpn. J. Appl. Phys.* **2011**, *50*, 04DK21.
(25) Li, G.; Shrotriya, V.; Yao, Y.; Yang, Y. *J. Appl. Phys.* **2005**, *98*, 043704.
(26) Gholamkhass, B.; Holdcroft, S. *Chem. Mater.* **2010**, *22*, 5371−5376.
(27) Izawa, S.; Hashimoto, K.; Tajima, K. *Phys. Chem. Chem. Phys.* **2012**, *14*, 16138−16142.
(28) Sivula, K.; Ball, Z. T.; Watanabe, N.; Frechet, J. M. J. *Adv. Mater.* **2006**, *18*, 206−210.
(29) Kim, B. J.; Miyamoto, Y.; Ma, B.; Fréchet, J. M. J. *Adv. Funct. Mater.* **2009**, *19*, 2273−2281.
(30) Miyanishi, S.; Zhang, Y.; Tajima, K.; Hashimoto, K. *Chem. Commun.* **2010**, *46*, 6723−6725.
(31) Yang, H. B.; Song, Q. L.; Gong, C.; Li, C. M. *Sol. Energy Mater. Sol. Cells* **2010**, *94*, 846−849.
(32) Xi, X.; Li, F.; Meng, Q.; Ding, Y.; Ji, J.; Shi, Z.; Li, G. *Sol. Energy Mater. Sol. Cells* **2010**, *94*, 924−929.
(33) Chen, D.; Liu, F.; Wang, C.; Nakahara, A.; Russell, T. P *Nano Lett.* **2011**, *11*, 2071−2078.
(34) Kim, H. J.; Han, A. .R.; Cho, C. H.; Kang, H.; Cho, H. H.; Lee, M. Y.; Frechet, J. M. J.; Oh, J. H.; Kim, B. J. *Chem. Mater.* **2012**, *24*, 215−221.
(35) Chen, F. C.; Ko, C. J.; Wu, J. L.; Chen, W. C. *Sol. Energy Mater. Sol. Cells* **2010**, *94*, 2426−2430.
(36) Yang, X.; Loos, J.; Veenstra, S. C.; Verhees, W. J. H.; Wienk, M. M.; Kroon, J. M.; Michels, M. A. J.; Janssen, R. A. J. *Nano Lett.* **2005**, *5*, 579−583.
(37) Moon, J. S.; Takacs, C. J.; Sun, Y.; Heeger, A. J. *Nano Lett.* **2011**, *11*, 1036−1039.
(38) Wang, D. H.; Moon, J. S.; Seifter, J.; Jo, J.; Park, J. H.; Park, O. O.; Heeger, A. J. *Nano Lett.* **2011**, *11*, 3163−3168.
(39) Savenije, T. J.; Kroeze, J. E.; Yang, X. N.; Loos, J. *Adv. Funct. Mater.* **2005**, *15*, 1260−1266.
(40) Wu, J. L.; Chen, F. C.; Hsiao, Y. S.; Chien, F. C.; Chen, P.; Kuo, C. H.; Huang, M. H.; Hsu, C. S. *ACS Nano* **2011**, *5*, 959−967.
(41) Hasobe, T.; Kamat, P. V.; Troiani, V.; Solladie, N.; Ahn, T. K.; Kim, S. K.; Kim, D.; Kongkanard, A.; Kuwabata, S.; Fukuzumi, S. *J. Phys. Chem. B* **2005**, *109*, 19−23.
(42) Hasobe, T.; Imahori, H.; Kamat, P. V.; Ahn, T. K.; Kim, S. K.; Kim, D.; Fujimoto, A.; Hirakawa, T.; Fukuzumi, S. *J. Am. Chem. Soc.* **2005**, *127*, 1216−1228.
(43) Emmi, S. S.; D'angelantonio, M.; Poggi, G.; Beggiato, G.; Camaioni, N.; Gerp, A.; Martelli, A.; Pietropaolo, D.; Zotti, G. *Res. Chem. Intermed.* **1998**, *24*, 1−14.
(44) Manceau, M.; Rivaton, A.; Gardette, J. L.; Guillerez, S.; Lemaître, N. *Polym. Degrad. Stab.* **2009**, *94*, 898−907.